This article has been accepted for publication in a future issue of this journal, but has not been fully edited. Content may change prior to final publication. Citation information: DOI 10.1109/TCSII.2018.2820104, IEEE Transactions on Circuits and Systems II: Express Briefs

Study of Amplitude Control and Dynamical Behaviors of a Memristive Band Pass Filter Circuit

Zbigniew Galias, *Senior Member, IEEE*

***Abstract*—The existence of a partial and total amplitude control in a band pass filter circuit with a memristor is explained theoretically and confirmed in simulations. A linear change of coordinates is derived to develop a simple three-parameter model of the circuit. Dynamical phenomena observed in the circuit are analyzed.**

I. Introduction

The existence of nonlinear circuit elements with resistance depending on the history of current flowing through the element or the voltage across the element has been postulated in [1]. The first memristor nano-device was reported in [2]. Since then memristors have received significant attention due to a number of possible applications including large capacity non-volatile memories and neuromorphic systems.

Understanding the dynamics of circuits containing memristors is a key step in the design of memristor-based networks [3], [4], [5], [6]. Recently, dynamical phenomena observed in memristor-based oscillators have been extensively studied. In most cases these oscillators contain memristors which are built using discrete components to mimic theoretical characteristics of ideal or extended memristors. A memristor emulator imitating the behavior of a TiO_2 memristor is presented in [7]. A floating analog memristor emulator circuit is proposed in [8]. A four dimensional memristor based chaotic circuit obtained by replacing the nonlinear element in the Chua's circuit with a memristor is studied in [3], [9]. The simplest chaotic memristor-based circuit containing an inductor, a capacitor and a memristor connected in series is studied in [10]. Further analysis of this circuit is carried out in [11], [12]. Dynamical phenomena in a floating memristor emulator based relaxation oscillator are analyzed in [13]. Memristive diode bridge with LCR filter is studied in [14]. Chaotic behaviors in a memristive Sallen-Key low pass filter are investigated in [15]. Numerical study of multiple attractors in the parallel inductor-capacitor-memristor circuit is carried out in [16].

A simple third-order memristive band pass filter circuit is introduced [17]. The authors carry out an analysis of its equilibria and their stability, construct bifurcation diagrams and observe the phenomenon of amplitude control.

Manuscript received Month ??, 2018; revised Month ??, 2018. This work was supported by the National Science Centre, Poland, grant no. 2015/17/B/ST7/03763.

The author is with the Department of Electrical Engineering, AGH University of Science and Technology, al. Mickiewicza 30, 30–059, Kraków, Poland, (e-mail: galias@agh.edu.pl).

Color versions of one or more of the figures in this paper are available online at http://ieeexplore.ieee.org.

Digital Object Identifier ??.????/????.????.???????

Amplitude control is an important property of dynamical systems in engineering applications since it permits adjusting amplitudes of generated signals to a desired level without the necessity of using amplifiers [18]. Recently, a considerable research effort has been devoted to the construction of systems and circuits with the mechanisms of total and partial amplitude control [19], [20].

In this work, the analysis of the third-order memristive band pass filter circuit introduced in [17] is continued. The mechanism of a partial amplitude control (PAC) is fully explained. Additionally, the property of a total amplitude control (TAC) is theoretically derived and confirmed in simulations. Using an appropriate linear change of variables a simple model of the circuit is constructed. The number of parameters in this model is reduced to three which considerably simplifies characterization of dynamical phenomena in the circuit. Analysis of the dynamics of the three-parameter model is carried out. A single-parameter bifurcation diagram is constructed, various dynamical phenomena are identified and the existence of observed attractors is confirmed using rigorous computational tools.

II. Third Order Memristive Band Pass Filter Circuit

The memristive band pass filter circuit [17] is shown in Fig. 1. It is built using an op-amp, two capacitors, three resistors and a memristor belonging to the class of extended voltage controlled memristors [21]. The dynamics of the memristor is defined by

$$i_1 = R_c^{-1}(1 - g v_0^2) v_1 \tag{1}$$

$$\dot{v}_0 = -(R_b C_0)^{-1} v_0 - (R_a C_0)^{-1} v_1, \tag{2}$$

where i_1, v_1, and v_0 are the memristor's current, voltage, and internal variable, respectively. An implementation of this memristor using two op-amps, three resistors, one capacitor, and two multipliers is described in [17].

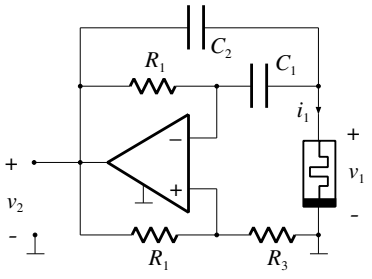

Fig. 1. The memristive band pass filter circuit.

1549-7747 (c) 2018 IEEE. Personal use is permitted, but republication/redistribution requires IEEE permission. See http://www.ieee.org/publications_standards/publications/rights/index.html for more information.

This article has been accepted for publication in a future issue of this journal, but has not been fully edited. Content may change prior to final publication. Citation information: DOI 10.1109/TCSII.2018.2820104, IEEE Transactions on Circuits and Systems II: Express Briefs

The dynamics of the circuit presented in Fig. 1 is defined by the following system of differential equations

$$\begin{aligned}\dot{v}_0 &= -(R_bC_0)^{-1}v_0 - (R_aC_0)^{-1}v_1,\\ \dot{v}_1 &= (1-gv_0^2)((k-1)R_cC_2)^{-1}v_1 - R_1^{-1}(C_1^{-1}+k^{-1}C_2^{-1})v_2,\\ \dot{v}_2 &= k(1-gv_0^2)((k-1)R_cC_2)^{-1}v_1 - R_1^{-1}(C_1^{-1}+C_2^{-1})v_2,\end{aligned} \quad (3)$$

where v_1 is the voltage across the memristor, v_2 is the voltage between the ground and the output of the operational amplifier, and $k = 1 + R_2/R_3$.

Using the notation $x = v_0$, $y = v_1$, $z = v_2$, rescaling time $\tau = t/(R_1C_1)$, and defining parameters $\alpha = C_2/C_1$, $\delta = (R_1C_2)/(R_bC_0)$, $\varrho = (R_1C_2)/(R_aC_0)$, $\varepsilon = R_1/R_c$ the circuit equations can be rewritten in the dimensionless form as

$$\begin{aligned}\dot{x} &= -\delta x - \varrho y,\\ \dot{y} &= \varepsilon(1-gx^2)(k-1)^{-1}y - (\alpha+k^{-1})z,\\ \dot{z} &= k\varepsilon(1-gx^2)(k-1)^{-1}y - (\alpha+1)z.\end{aligned} \quad (4)$$

Behavior of the system depends on six parameters: δ, ϱ, g, k, ε and α. In [17], the authors assume that $C_1 = C_2$. Under this assumption the parameter α is equal to 1, and the number of parameters is reduced to five. Analysis of the system (4) is carried out in [17] for the case in which four parameters are fixed $\alpha = 1$, $\varepsilon = 500/3$, $g = 0.1$, $k = 21$ and the parameters δ and ϱ are varied. Bifurcation diagrams are constructed and Lyapunov exponents are computed.

In [17], the authors compute equilibria and characteristic equations of Jacobian matrices of (4) at equilibria finding out that the characteristic equations do not depend on the parameter ϱ. They conclude that it follows that "the dynamical characteristic of system (4) has nothing to do with the parameter ϱ". This explanation is not valid. Jacobian matrices at equilibria define dynamical behaviors in neighborhoods of equilibria. Properties of the global dynamics of the system cannot be concluded from the analysis of local behavior around equilibria alone. The authors notice that when other parameters are fixed, changing the parameter ϱ rescales attractors in such a way that amplitudes of variables y and z are proportional to ϱ, while the amplitude of x does not change. They are however not able to explain this phenomenon and write "However, if the transformation $(x, y, z) \mapsto (x, y/\varrho, z/\varrho)$ is performed, the algebraic system structure will change".

III. Amplitude Control Mechanisms

In this section, we explain the phenomenon of variables' rescaling. It will be shown that rescaling variables in a proper way produces systems with different values of ϱ and other parameters unchanged. We also show that the system has the property of a total amplitude control, in which all variables can be rescaled by the modification of a single parameter of the circuit.

First, let us notice that introducing the variable change $(x, y, z) \mapsto (x, \eta y, \eta z)$ converts (4) to the following dynamical system

$$\begin{aligned}\dot{x} &= -\delta x - \eta^{-1}\varrho y,\\ \dot{y} &= \varepsilon(1-gx^2)(k-1)^{-1}y - (\alpha+k^{-1})z,\\ \dot{z} &= k\varepsilon(1-gx^2)(k-1)^{-1}y - (\alpha+1)z.\end{aligned} \quad (5)$$

The only change is in the coefficient at the y variable in the first equation. This coefficient changes from ϱ to $\eta^{-1}\varrho$. It follows that two systems (4) with different values of ϱ are equivalent from the dynamical point of view. More precisely, the system (4) with parameter ϱ_1 is converted to the system with parameter ϱ_2 if the transformation $(x, y, z) \mapsto (x, \varrho_1\varrho_2^{-1}y, \varrho_1\varrho_2^{-1}z)$ is applied. Modifying the parameter ϱ is equivalent to appropriate rescaling of variables y and z while the variable x is not changed. The parameter ϱ can be used for the partial amplitude control (PAC), where modifying a single parameter rescales amplitudes of selected variables, while amplitudes of other variables are not altered [18].

Now, we will show how to simultaneously rescale all variables in the system (4) by changing a single parameter. This is called a total amplitude control (TAC) [18]. In TAC, it is required that the right-hand side of the equation defining the dynamical system contain terms which are all monomials of the same degree apart from the one, whose coefficient can be used for amplitude control. The system (4) contains six linear terms and two nonlinear terms. However, the nonlinear terms are of the same degree and both contain the parameter g, which is not present in other terms. This makes a total amplitude control for the system (4) possible. Let us consider the following variable change $(x, y, z) \mapsto (sx, sy, sz)$, where s is the factor scaling proportionally all variables. Applying this coordinate change to (4) yields

$$\begin{aligned}\dot{x} &= -\delta x - \varrho y,\\ \dot{y} &= \varepsilon(1-s^{-2}gx^2)(k-1)^{-1}y - (\alpha+k^{-1})z,\\ \dot{z} &= k\varepsilon(1-s^{-2}gx^2)(k-1)^{-1}y - (\alpha+1)z.\end{aligned} \quad (6)$$

The difference between (4) and (6) is that g is replaced by g/s^2. It follows that decreasing g by the factor s scales trajectories by the factor $\sqrt{s}$ in all variables. The amplitudes of all variables may be controlled by changing g. This is an example of a total amplitude control [18].

Results regarding amplitude control are confirmed in simulations. Fig. 2(a) shows a trajectory of the system (4) with parameters $\delta = 8$, $\varrho = 80$, $\varepsilon = 500/3$, $g = 0.1$, $k = 21$, and $\alpha = 1$ with the initial condition $(x_0, y_0, z_0) = (0.1, 0, 0.1)$. Results of the partial amplitude control are shown in Fig. 2(b), where ϱ is decreased by a factor 2 and the initial condition is rescaled in the y and z variables $(x_0, y_0, z_0) = (0.1, 0, 0.2)$. One can see that the plot is the same as in Fig. 2(a) with the only difference in the amplitude of the y variable, which is two times larger. Similarly, the amplitude of the z variable is increased two times. Results of the total amplitude control are shown in Fig. 2(c), where g is increased four times and the initial condition is rescaled in all variables to $(x_0, y_0, z_0) = (0.05, 0, 0.05)$. As a result of the total amplitude control amplitudes of all variables are decreased by a factor 2. This is consistent with the results of theoretical analysis in which we showed that the scaling factor of the amplitudes is inversely proportional to the square of the scaling factor of g.

In the original definition of a total and partial amplitude control, a single parameter is used to rescale all or some of the system's variables [18]. Here, we demonstrate how to obtain the partial amplitude control of x by a simultaneous

1549-7747 (c) 2018 IEEE. Personal use is permitted, but republication/redistribution requires IEEE permission. See http://www.ieee.org/publications_standards/publications/rights/index.html for more information.

This article has been accepted for publication in a future issue of this journal, but has not been fully edited. Content may change prior to final publication. Citation information: DOI 10.1109/TCSII.2018.2820104, IEEE Transactions on Circuits and Systems II: Express Briefs

modification of two parameters. Independent rescaling of the amplitude of the x variable can be achieved by changing both ϱ and g. This is illustrated in Fig. 2(d), where ϱ is decreased by a factor 2, g is increased four times when compared to the first case, and the initial condition is rescaled in the x variable to $(x_0, y_0, z_0) = (0.05, 0, 0.1)$. As a result in this case the amplitude of x is decreased by a factor 2, while the amplitudes of y and z are unaltered.

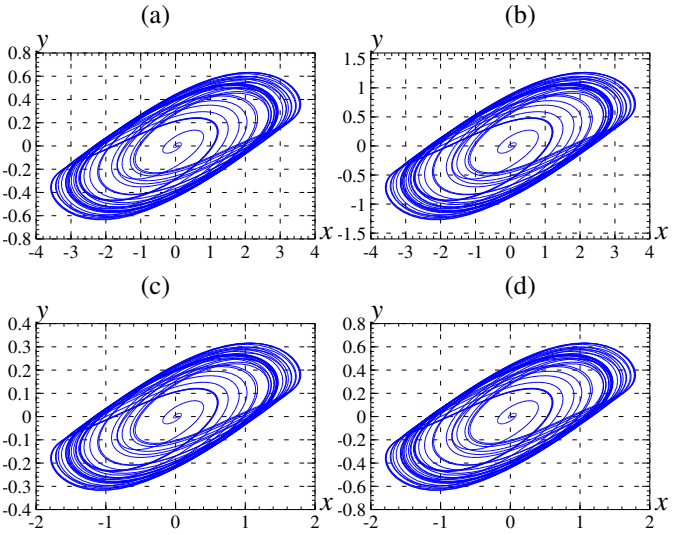

Fig. 2. Trajectories of (4) with $\delta = 8$, $\varepsilon = 500/3$, $k = 21$, and $\alpha = 1$; (a) $\varrho = 80$, $g = 0.1$, (b) $\varrho = 40$, $g = 0.1$, (c) $\varrho = 80$, $g = 0.4$, (d) $\varrho = 40$, $g = 0.4$.

Fig. 3 shows the amplitudes of signals generated by the circuit in the total and partial amplitude control. In TAC, g is the control parameter. Other parameters are fixed at $\delta = 8$, $\varepsilon = 500/3$, $k = 21$, $\alpha = 1$, and $\varrho = 80$. 101 values of the parameter g selected uniformly in the interval $g \in [0.05, 0.2]$ are considered. For each value, a steady state trajectory starting from initial conditions $(x_0, y_0, z_0) = (0.1, 0, 0.1)$ is found. Note that here, we do not rescale the initial conditions. Nevertheless, the steady-state is the the same because in this case a single attractor is observed in simulations. The minimum and the maximum value of each variable in the steady-state are plotted in Fig. 3(a). The extremal values of x, y, and z variables are plotted in blue, red and magenta, respectively. The parameter value $g = 0.1$ corresponding to Fig. 2(a) is denoted as a gray vertical line. The amplitudes of all variables are inversely proportional to the square root of g.

In the partial amplitude control the parameter ϱ is changed. Computations are carried out for 101 values belonging to the interval $\varrho \in [40, 160]$. The minimum and the maximum value of each variable in the steady-state are plotted in Fig. 3(b). The amplitude of x is not influenced by PAC, while the amplitudes of remaining variables are inversely proportional to ϱ.

Since Lyapunov exponents are invariant under a linear change of coordinates [22], it is clear that the Lyapunov exponent spectrum is not altered by changing ϱ and g.

Amplitude control may be useful in applications in which signals with predefined amplitudes are required. Note that ϱ is inversely proportional to R_a and that R_a is not present in

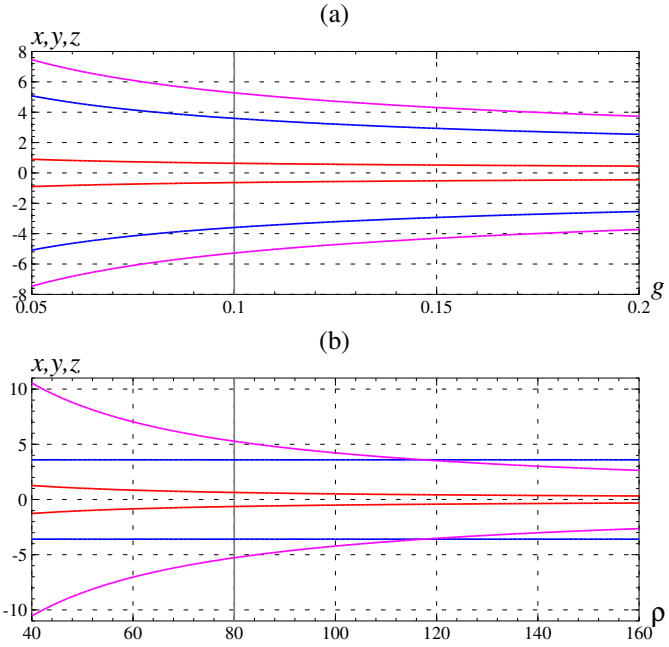

Fig. 3. Amplitudes of variables versus control parameter: (a) the total amplitude control, (b) the partial amplitude control.

the definitions of δ, ε, k, and α. Hence, as noticed in [17], the amplitudes of signals generated by the circuit can be adjusted by a potentiometer at the element R_a. Changing R_a causes PAC regarding voltages v_1 and v_2. The total amplitude control resulting in a uniform scaling of all voltages v_0, v_1, and v_2 is achieved by the modification of the parameter g of the memristor.

IV. A Three Parameter Model of the Circuit

From the discussion presented in the previous section it follows that systems (4) with different values of the parameters ϱ and g are equivalent from the dynamical point of view (Lyapunov spectrum is the same, solutions and attractors are simply rescaled). It is sufficient to study system's behaviors for single values of these parameters, for example $\varrho = 1$, $g = 1$. Hence, we can eliminate two parameters of the system (4) by a linear change of coordinates. Yet another parameter can be eliminated by using an appropriate time rescaling.

Below, we derive a linear transformation reducing the number of parameters to three and simplifying the differential equations defining the dynamical system so that it contains a single nonlinear term. Let us define new variables $x = -v_0/s$, $y = v_1 R_b/(sR_a)$, $w = v_2 R_b/(skR_a)$, $\tau = t/(R_b C_0)$, where s is a scaling factor. The value of s will be selected later. In these new variables the dynamical system (3) can be rewritten as

$$\begin{aligned} \frac{\mathrm{d}x}{\mathrm{d}\tau} &= -x + y, \\ \frac{\mathrm{d}y}{\mathrm{d}\tau} &= \frac{R_b C_0 (1 - g s^2 x^2)}{(k-1) R_c C_2} y - \frac{R_b C_0 (k\alpha + 1)}{R_1 C_2} w, \\ \frac{\mathrm{d}w}{\mathrm{d}\tau} &= \frac{R_b C_0 (1 - g s^2 x^2)}{(k-1) R_c C_2} y - \frac{R_b C_0 (\alpha + 1)}{R_1 C_2} w. \end{aligned} \tag{7}$$

Note that nonlinear terms in (7) are identical. This allows us to simplify differential equations by eliminating one of the

1549-7747 (c) 2018 IEEE. Personal use is permitted, but republication/redistribution requires IEEE permission. See http://www.ieee.org/publications_standards/publications/rights/index.html for more information.

This article has been accepted for publication in a future issue of this journal, but has not been fully edited. Content may change prior to final publication. Citation information: DOI 10.1109/TCSII.2018.2820104, IEEE Transactions on Circuits and Systems II: Express Briefs

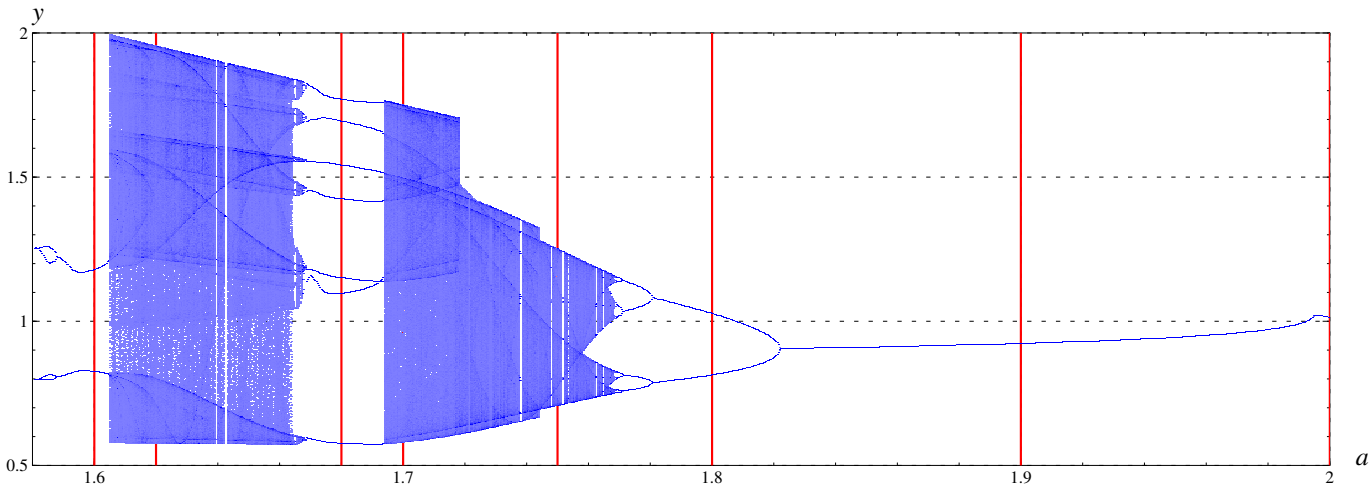

Fig. 4. Bifurcation diagram of the system (9) for $a \in [1.58, 2]$, $b = 2.75$, $c = 2.5$.

nonlinear terms. Let use define a new variable $z = y - w$. Equations (7) in variables (x, y, z) can be written as

$$\begin{aligned} \dot{x} &= -x + y, \\ \dot{y} &= -ay + bz - ds^2x^2y, \\ \dot{z} &= c(z - y), \end{aligned} \tag{8}$$

where $a = R_bC_0(k\alpha + 1)/(R_1C_2) - R_bC_0/((k-1)R_cC_2)$, $b = R_bC_0(k\alpha + 1)/(R_1C_2)$, $c = R_bC_0(k-1)/(R_1C_1)$, and $d = gR_bC_0/((k-1)R_cC_2)$. Note that for positive R_2, R_3, R_c, C_2, R_b, C_0, and g, the parameters b, c, d and the difference $b - a$ are always positive.

Let us select the scaling factor s in such a way that the coefficient at x^2y in the second equation is equal to -1, i.e. $s = \sqrt{d^{-1}} = \sqrt{(k-1)R_cC_2/(gR_bC_0)}$. This is always possible since d is positive. For this selection, we obtain a dynamical system with three parameters

$$\begin{aligned} \dot{x} &= -x + y, \\ \dot{y} &= -ay + bz - x^2y, \\ \dot{z} &= c(z - y). \end{aligned} \tag{9}$$

Reducing the number of parameters from six for the model (4) to three for the model (9) simplifies the process of studying dynamical phenomena in the system.

V. Analysis of the Three Parameter Model

In this section, we analyze dynamical phenomena in the three parameter model derived in the previous section.

Let us note that the system (9) is symmetric with respect to the transformation $(x, y, z) \mapsto (-x, -y, -z)$. It follows that if $(x(t), y(t), z(t))$ is a trajectory of (9) then also is $(-x(t), -y(t), -z(t))$. As a consequence there might exist two types of steady-state solutions: self-symmetric solutions and symmetric pairs of solutions.

If $(b - a)$ is positive the system possesses three equilibria $(0, 0, 0)$, and $\pm x^\star = (\pm x_1^\star, \pm x_1^\star, \pm x_1^\star)$, where $x_1^\star = \sqrt{b-a}$. Since $b - a = R_bC_0/((k-1)R_cC_2) > 0$ it follows that there are always three equilibria of the original system (3).

In the following, we carry out a bifurcation analysis of the system (9), with a being the bifurcation parameter and other parameters fixed at $b = 2.75$, $c = 2.5$. A bifurcation diagram of the y variable at the intersection of trajectories with the plane $x = 0$ is shown in Fig. 4. One can see various dynamical phenomena including period-doubling bifurcations, chaotic regions and periodic windows.

Attractors existing for selected values of a are shown in Fig. 5. Initial points are selected as $(x_0, y_0, z_0) = (\pm 0.1, 0, \pm 0.1)$. To avoid transients, in each case a trajectory of the length $T = 1000$ is computed and its second half is plotted. In cases when a symmetric pair of attractors coexists, attractors are plotted using different colors. The attractors reached from the initial points $(0.1, 0, 0.1)$ and $(-0.1, 0, -0.1)$ are plotted in blue and red respectively. For $a = 2$ there exists a stable self-symmetric periodic orbit [see Fig. 5(a)]. For $a \approx 1.995$ this orbit loses stability and a symmetric pair of stable periodic orbits is born [see Fig. 5(b)]; one of the branches can be seen in the bifurcation plot. When a is decreased this periodic orbit undergoes a period doubling bifurcation for $a \approx 1.823$ [compare Fig. 5(c)]. For $a < 1.823$, there is a sequence of period-doubling bifurcations which leads to a chaotic behavior. A symmetric pair of chaotic attractors exists roughly for $a > 1.72$. An example is shown in Fig. 5(d). At $a \approx 1.72$ chaotic attractors collide and a self-symmetric chaotic attractor is born [compare Fig. 5(e) and (g)]. Periodic windows exist within the chaotic region. The stable self-symmetric periodic orbit existing for $a = 1.68$ is shown in Fig. 5(f). The chaotic region exists approximately for $a > 1.605$. For $a < 1.605$ a symmetric pair of periodic attractors exists [see Fig. 5(h)].

The existence of attractors is confirmed using interval arithmetic tools [23]. Computations in interval arithmetic are carried out in such a way that a proper rounding is used when calculating bounds of mathematical expressions. In this way results returned by a computer always enclose the true results and we can be sure that phenomena observed in computations are not rounding error artifacts [24], [25]. The existence of attractors is studied by applying interval tools to the return map defined by the section $\{(x, y, z)\colon x = 0\}$. The return map

1549-7747 (c) 2018 IEEE. Personal use is permitted, but republication/redistribution requires IEEE permission. See http://www.ieee.org/publications_standards/publications/rights/index.html for more information.

This article has been accepted for publication in a future issue of this journal, but has not been fully edited. Content may change prior to final publication. Citation information: DOI 10.1109/TCSII.2018.2820104, IEEE Transactions on Circuits and Systems II: Express Briefs

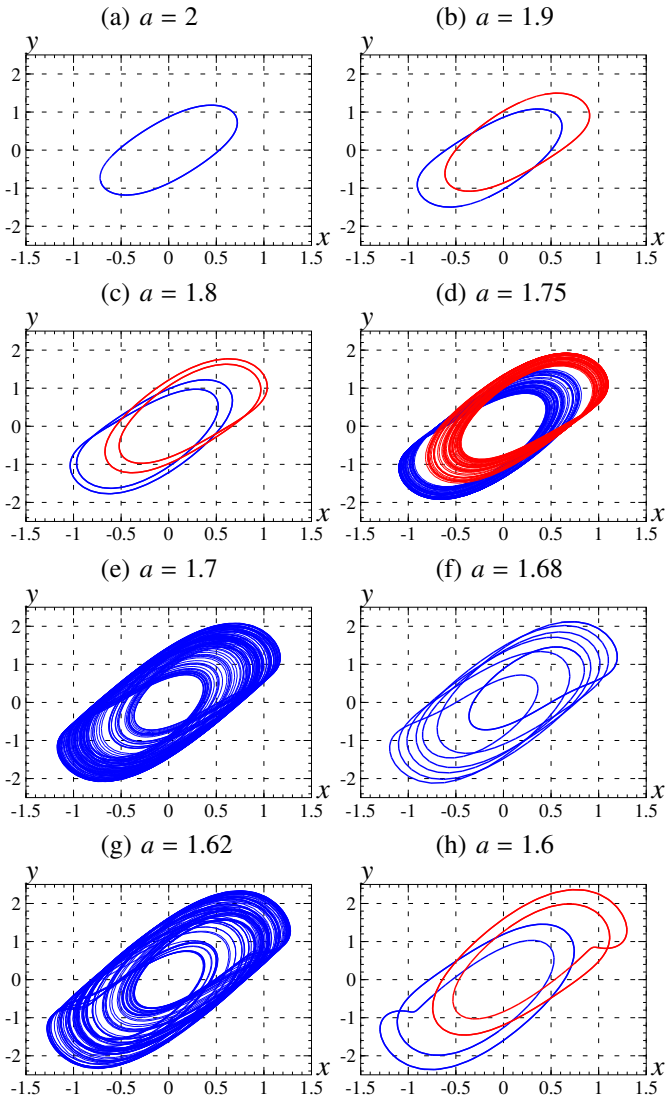

Fig. 5. Attractors existing for selected values of parameter a; $a \in \{2.0, 1.9, 1.8, 1.75, 1.7, 1.68, 1.62, 1.6\}$, $b = 2.75$, $c = 2.5$. Initial points $(x_0, y_0, z_0) = (\pm 0.1, 0, \pm 0.1)$.

P and its derivative are rigorously evaluated using the CAPD library [26]. The existence of all periodic attractors shown in Fig. 5 is verified using the interval Newton method [27]. In case of chaotic attractors, the existence of infinitely many periodic orbits and chaotic trajectories is confirmed using the method of covering relations [28], [25]. Computational details are skipped for the sake of brevity.

VI. Conclusions

It has been shown that a memristive band pass filter circuit possesses a total and partial amplitude control mechanisms. In the total amplitude control by changing the value of one of the circuit's parameters the amplitudes of all variables are rescaled by the same factor. In the partial amplitude control the amplitude of one of the variables remains constant while the others are rescaled by the same factor. A linear change of coordinates has been constructed in such a way that the behavior of the resulting dynamical system depends on three parameters only. Dynamical phenomena of this system have been studied.

References

[1] L. O. Chua, "Memristor: The missing circuit element," *IEEE Trans. Circ. Theory*, vol. 18, no. 5, pp. 507–519, 1971.
[2] D. B. Strukov, G. S. Snider, D. R. Stewart, and R. S. Williams, "The missing memristor found," *Nature*, vol. 453, pp. 80–83, 2008.
[3] M. Itoh and L. O. Chua, "Memristor oscillators," *Int. J. Bifurcation Chaos*, vol. 18, pp. 3183–3206, 2008.
[4] F. Corinto, A. Ascoli, and M. Gilli, "Nonlinear dynamics of memristor oscillators," *IEEE Trans. Circuits Systems I*, vol. 58, no. 6, pp. 1323–1336, 2011.
[5] R. Riaza, "First order mem-circuits: Modeling, nonlinear oscillations and bifurcations," *IEEE Trans. Circuits Systems I*, vol. 60, no. 6, pp. 1570–1583, 2013.
[6] M. Itoh and L. O. Chua, "Dynamics of memristor circuits," *Int. J. Bifurcation Chaos*, vol. 24, no. 5, p. 1430015, 2014.
[7] H. Kim, M. P. Sah, C. Yang, S. Cho, and L. O. Chua, "Memristor emulator for memristor circuit applications," *IEEE Trans. Circ. Syst. I*, vol. 59, no. 10, pp. 2422–2431, 2012.
[8] C. Sánchez-López, J. Mendoza-López, M. Carrasco-Aguilar, and C. Muniz-Montero, "A floating analog memristor emulator circuit," *IEEE Trans. Circ. Syst. II*, vol. 61, no. 5, pp. 309–313, 2014.
[9] H. H. C. Iu, D. S. Yu, A. L. Fitch, V. Sreeram, and H. Chen, "Controlling chaos in a memristor based circuit using a twin-T notch filter," *IEEE Trans. Circ. Syst. I*, vol. 58, no. 6, pp. 1337–1344, 2011.
[10] B. Muthuswamy and L. Chua, "Simplest chaotic circuit," *Int. J. Bifurcation and Chaos*, vol. 20, no. 5, pp. 1567–1580, 2010.
[11] Y. Zhang and X. Zhang, "Dynamics of the Muthuswamy-Chua system," *Int. J. Bifurcation and Chaos*, vol. 23, no. 8, p. 1350136 (7 pages), 2013.
[12] Z. Galias, "Automatized search for complex symbolic dynamics with applications in the analysis of a simple memristor circuit," *Int. J. Bifurcation Chaos*, vol. 24, no. 7, p. 1450104 (11 pages), 2014.
[13] D. Yu, H. H. C. Iu, A. L. Fitch, and Y. Liang, "A floating memristor emulator based relaxation oscillator," *IEEE Trans. Circ. Syst. I*, vol. 61, no. 10, pp. 2888–2896, 2014.
[14] F. Corinto and A. Ascoli, "Memristive diode bridge with LCR filter," *Electronics Letters*, vol. 48, no. 14, pp. 824–825, 2012.
[15] B. C. Bao, P. Wu, H. Bao, M. Chen, and Q. Xu, "Chaotic bursting in memristive diode bridge-coupled Sallen-Key lowpass filter," *Electronics Letters*, vol. 53, no. 16, pp. 1104–1105, 2017.
[16] Z. Galias, "Numerical study of multiple attractors in the parallel inductor-capacitor-memristor circuit," *Int. J. Bifurcation Chaos*, vol. 27, no. 11, p. 1730036 (16 pages), 2017.
[17] B. Bao, N. Wang, Q. Xu, H. Wu, and Y. Hu, "A simple third-order memristive band pass filter chaotic circuit," *IEEE Trans. Circ. Syst. II*, vol. 64, no. 8, pp. 997–981, 2017.
[18] C. Li and J. Sprott, "Amplitude control approach for chaotic signals," *Nonlinear Dynamics*, vol. 73, no. 3, pp. 1335–1341, 2013.
[19] C. Li, J. C. Sprott, W. Thio, and H. Zhu, "A new piecewise linear hyperchaotic circuit," *IEEE Trans. Circuits Syst. II*, vol. 61, no. 12, pp. 977–981, 2014.
[20] C. Li, J. C. Sprott, Z. Yuan, and H. Li, "Constructing chaotic systems with total amplitude control," *Int. J. Bifurcation Chaos*, vol. 25, no. 10, p. 1530025 (14 pages), 2015.
[21] L. O. Chua, "The fourth element," *Proc. IEEE*, vol. 100, no. 6, pp. 1920–1927, 2012.
[22] N. V. Kuznetsov, T. A. Alexeeva, and G. A. Leonov, "Invariance of Lyapunov exponents and Lyapunov dimension for regular and irregular linearizations," *Nonlinear Dynamics*, vol. 85, no. 1, pp. 195–201, 2016.
[23] R. Moore, *Methods and applications of interval analysis*. Philadelphia: SIAM, 1979.
[24] R. Lozi, "Can we trust in numerical computations of chaotic solutions of dynamical systems?" in *Topology and Dynamics of Chaos*, C. Letellier and R. Gilmore, Eds. World Scientific, 2013, vol. 84, pp. 29–64.
[25] Z. Galias, "The dangers of rounding errors for simulations and analysis of nonlinear circuits and systems — and how to avoid them," *IEEE Circuits Syst. Mag.*, vol. 13, no. 3, pp. 35–52, 2013.
[26] "CAPD library," http://capd.ii.uj.edu.pl/, 2016.
[27] A. Neumaier, *Interval Methods for Systems of Equations*. Cambridge, UK: Cambridge University Press, 1990.
[28] P. Zgliczyński, "Computer assisted proof of chaos in the Rössler equations and in the Hénon map," *Nonlinearity*, vol. 10, no. 1, pp. 243–252, 1997.

1549-7747 (c) 2018 IEEE. Personal use is permitted, but republication/redistribution requires IEEE permission. See http://www.ieee.org/publications_standards/publications/rights/index.html for more information.